

Nucleation dynamics in two-dimensional cylindrical Ising models and chemotaxis

C. Bosia,^{1,2,*} M. Caselle,^{1,2,†} and D. Corá^{3,2,‡}¹*Dipartimento di Fisica Teorica, Università di Torino and INFN, via P. Giuria 1, I-10125 Torino, Italy*²*Center for Complex Systems in Molecular Biology and Medicine, University of Torino, Via Accademia Albertina 13, I-10100 Torino, Italy*³*Systems Biology Lab, Institute for Cancer Research and Treatment (IRCC), School of Medicine, Università di Torino, Str. Prov. 142, Km. 3.95, Candiolo I-1060 Torino, Italy*

(Received 5 August 2009; revised manuscript received 15 October 2009; published 8 February 2010)

The aim of our work is to study the effect of geometry variation on nucleation times and to address its role in the context of eukaryotic chemotaxis (i.e., the process which allows cells to identify and follow a gradient of chemical attractant). As a first step in this direction we study the nucleation dynamics of the two-dimensional Ising model defined on a cylindrical lattice whose radius changes as a function of time. Geometry variation is obtained by changing the relative value of the couplings between spins in the compactified (vertical) direction with respect to the horizontal one. This allows us to keep the lattice size unchanged and study in a single simulation the values of the compactification radius which change in time. We show both with theoretical arguments and numerical simulations that squeezing the geometry allows the system to speed up nucleation times even in presence of a very small energy gap between the stable and the metastable states. We then address the implications of our analysis for directional chemotaxis. The initial steps of chemotaxis can be modeled as a nucleation process occurring on the cell membrane as a consequence of the external chemical gradient (which plays the role of energy gap between the stable and metastable phases). In nature most of the cells modify their geometry by extending quasi-one-dimensional protrusions (filopodia) so as to enhance their sensitivity to chemoattractant. Our results show that this geometry variation has indeed the effect of greatly decreasing the time scale of the nucleation process even in presence of very small amounts of chemoattractants.

DOI: [10.1103/PhysRevE.81.021907](https://doi.org/10.1103/PhysRevE.81.021907)

PACS number(s): 87.17.Jj, 64.60.De, 64.60.My, 64.60.Q–

I. INTRODUCTION

The decay of the metastable state at a first-order phase transition is a rather well-understood problem both in statistical mechanics and in quantum field theory (QFT). It attracted much interest in these last years due to its role in various different physical contexts ranging from the condensed-matter applications to the study of the deconfinement transition in quantum chromodynamics (QCD) or of the inflationary mechanism in cosmology. The crucial problem in all these contexts is the evaluation of the lifetime of the metastable state from the knowledge of the microscopic interactions of the system and of the details of the nonequilibrium dynamics which drives it toward the true equilibrium state. If the Hamiltonian of the system only contains short-range interactions then, as a general result, metastable states will always decay but their lifetime can vary by orders of magnitude. A simple but powerful effective model for the description of metastable decay is the so-called droplet model which traces back to the seminal papers by Becker and Döring and Zeldovich [1,2] and was later reinterpreted and extended using a field-theoretic language by Langer and Coleman and Callan [3–5] (for a review see for instance [6]). The main result of this approach is that the lifetime of the metastable state depends exponentially on the free energy F_c of the so-called “critical droplet” whose size R_c can be evalu-

ated by comparing the bulk and perimeter contributions to the free energy of the droplet. The weak metastability regime (in which we are interested in this paper) is reached when the F_c is much larger than the temperature of the system (or than the Plank’s constant in field theoretic applications).

In this “classical” framework the system is assumed to be of infinite extension and the background space-time geometry is assumed to be flat and fixed. The picture becomes much more interesting if these two constraints are relaxed. When the system has a finite size L , comparable with the critical radius R_c , then the competition between these two scales may induce very different behaviors and creates a combination of different dynamical regimes [7]. In particular for $L \ll R_c$, the limiting scale of the nucleation process becomes the ratio L/ξ , where ξ is the bulk correlation length of the system. When the background geometry is allowed to fluctuate then the exponential regime itself is abrogated and one finds instead a power-law dependence of the decay rate [8] on the energy gap.

The aim of our paper is to show, following the above observations, that by acting on the background geometry one can indeed modify the decay rate of the system and reach even for very small energy gaps between the stable and metastable phases, very short values for the lifetime of the metastable phase.

Besides its intrinsic interest, this feature may be of some importance for biological applications. Nucleation theory, among several other biological applications, plays an important role in eukaryotic chemotaxis (the process which allows eukaryotic cells to identify and follow a gradient of chemical attractant). Chemotaxis is mediated by two key enzymes: phosphatidylinositol three-kinase (PI3K) and phosphatase

*cbosia@to.infn.it

†caselle@to.infn.it

‡davide.cora@ircc.it

and tensin-homolog (PTEN). The standard way to model the process is to assume that the cell membrane, as a consequence of the external chemical gradient, undergoes a phase ordering process reaching a stable phase-separation regime between a PI3K-rich phase (toward the chemoattractant) and a PTEN-rich phase (opposite to the chemoattractant) [9–11]. In this picture the chemical gradient plays the role of energy gap between the stable and metastable phases. The limiting scale of this process is the cell size. Gradients smaller than a critical value would require critical droplets larger than the cell size to drive the process and this would lead, depending on the details of the model, to a random orientation of the two phases or to a dramatic increase in the time scale of the process. The way cells adopt to overcome this problem and enhance their sensitivity to chemoattractant is to modify their geometry by extending quasi-one-dimensional (1D) protrusions (filopodia). This change in background geometry is exactly the type of process that we plan to study in this paper.

All along the paper we shall use the two-dimensional (2D) Ising model as prototypical example of a statistical system with short-range interactions showing metastable phases when an external magnetic field is applied in the broken symmetry phase of the model. Besides this paradigmatic role there are two other important reasons which led us to concentrate in the Ising model.

The first one is that it has been recently shown in [12] that the chemotacting model described above can be mapped into a suitable generalization of the 2D Ising model. The standard Ising model is obtained in the limit of infinite amount of cytosolic PTEN and PI3K enzymes (we shall discuss this mapping in some details below).

The second reason is somehow more technical but of similar importance for our purposes. The 2D Ising model can be exactly solved (and the correlation length can be exactly evaluated) even for asymmetric values of the coupling constants. This fact will play a crucial role in the protocol that we shall use to modify the background geometry of the model. In fact it will allow us to modify the geometry by simply acting on the coupling constants of the model without changing the structure of the 2D lattice (which would require a very sophisticated and inefficient software).

This paper is organized as follows. In Sec. II we shall briefly discuss the chemotacting model mentioned above. In Sec. III we shall introduce the Ising model with asymmetric couplings and briefly discuss its phase diagram. Section IV will be devoted to a brief review of the classical nucleation theory (CNT) with a particular attention to the interplay between the two main scales of the problem: the system size L and the critical droplet radius R_c . In Sec. V we shall discuss the procedure we adopted to vary the geometry of the system and the results of our simulations while the last section will be devoted to a few concluding remarks.

II. SIMPLE CHEMOTACTING MODEL AND ITS ISING-LIKE REALIZATION

The link between nucleation dynamics in 2D Ising models and chemotaxis is based on the observation that chemotaxis requires as a preliminary step a phase-separation process on the membrane of the cell [9–11].

When a chemoattractant is switched on in the external environment of the cell, owing to the interplay of the two enzymes PTEN and PI3K, the phospholipids phosphatidylinositol biphosphate (PIP₂) and phosphatidylinositol trisphosphate (PIP₃) are interconverted: PI3K catalyzes PIP₂ phosphorylation and PTEN catalyzes PIP₃ dephosphorylation. While the phospholipids are bound to the inner surface of the membrane, the enzymes can freely diffuse in the cytoplasm, becoming active if absorbed on the membrane. When it happens, it is observed the formation of two patches in complementary domains, rich in PIP₂ and PIP₃, respectively. In particular, the PIP₃-rich patch is localized on the side of the membrane exposed to the highest concentration of chemoattractant (the leading edge) while the PIP₂ rich-one on the other side (the rear edge). Similarly, a phase separation also involves cytoplasmic localization of the enzymes PI3K and PTEN.

Such spatial-organization phenomenon may be seen as a self-organized phase ordering process, where the cell state—driven by an external field—decays into two spatially localized chemical phases, thus defining a front and a rear. This process lies at the heart of directional sensing, finally leading to cell movement toward the maximum of the attractant gradient.

Following [12] the dynamics of the phase-separation process occurring in the cell membrane can be modeled with a suitable generalization of the 2D Ising model. The cell membrane is represented by a square lattice of side L with periodic boundary conditions and the spin variables $S_i = +1(-1)$ are the enzymes PI3K (PTEN). The Hamiltonian of the model is composed by three terms: a short-range (i.e., involving nearest-neighborhood sites) ferromagnetic coupling describing the attractive interaction between enzymes, an external site-dependent magnetic field mapping the effect of the attractant and a long-range antiferromagnetic interaction term which keeps into account the finiteness of the cytosolic enzymatic reservoir.

From the ratio of probabilities that PI3K and PTEN enzymes bind to the site i , it is possible to trace the energy difference between states $S_i = +1$ and $S_i = -1$,

$$\Delta H = -2J \sum_{j \in \partial i} S_j - 2h_i + 2\lambda m \quad (1)$$

(where $j \in \partial i$ are the j nearest-neighborhood sites of the site i) which can be reinterpreted as the variation in the Hamiltonian

$$H = -J \sum_{\langle i,j \rangle} S_i S_j - \sum_i h_i S_i + \frac{\lambda}{N} \sum_{i < j} S_i S_j, \quad (2)$$

where J is the ferromagnetic coupling constant, the first sum is over all the nearest-neighborhood sites ($\langle i,j \rangle$), h_i is the external site-dependent field representing the chemoattractant, N is the total number of enzymes PTEN and PI3K and λ is a constant weighing the antiferromagnetic term with respect to the ferromagnetic one. The standard Ising model is recovered in the $N \rightarrow \infty$ limit, i.e., for an infinite enzymatic reservoir. However it is important to stress that this is a non-trivial limit. In fact due to the additional antiferromagnetic

term the generalized 2D Ising model behaves in a quite different way with respect to the standard Ising model. In the broken symmetry phase it shows self-tuned phase separations also for very small amounts of gradient. However if the gradient is too small the two phases are randomly distributed on the lattice (i.e., the cell membrane) and chemotaxis cannot occur. In this generalized Ising model the absence of correlation between the spatial orientation of the two phases and the external field plays the role of the exponential increase in the metastable state lifetime in the standard Ising model. In this paper we decided to concentrate in the $N \rightarrow \infty$ Ising limit since it allows a rigorous theoretical description. We plan to devote a forthcoming paper to a detailed numerical analysis of its finite N generalization.

In the above model the geometry plays no role: the lattice is a flat two-dimensional torus which is assumed to be a reasonable approximation of a spherical cell membrane. However this is a very crude approximation from a biological point of view. Indeed in the chemotactic process, the geometry of the cell plays a pivotal role: signal sensing takes place as the leading edges of nearly one-dimensional finger-like projections (called *filopodia*) protrude from the cellular body. Such structures, as sophisticated antennas, allow the cell to sense even subtle concentrations of external signal, finally enabling motion (see [13–15]). Since filopodia are dynamic structures appearing to sense the signal when the source of chemoattractant is far from the cell, the membrane is continually forced to change its geometry, squeezing and splitting its leading edge. Moreover, since in a nearly one-dimensional geometry the interface tension between two different phases is lower than in a spherical geometry, even a very small gradient of external field can drive the coarsening toward its maximum. If the geometry fluctuates, the thin fingers developed from the leading edge can sense small amounts of gradient thanks to the rapid formation of clusters rich in PIP₃ in the free extremities (and PIP₂ in their complementary share) and then maintain the phase separation in the spherical geometry once they are reabsorbed by the membrane.

As mentioned in the introduction the main goal of our work is to try to include these effects in the model by simulating the formation of a quasi-one-dimensional filopodium and then its reabsorption within the cell membrane.

III. ISING MODEL WITH ASYMMETRIC COUPLINGS

A. General setting

The 2D Ising model with asymmetric couplings is defined by the following Hamiltonian [16]:

$$H = -J_x \sum_{\langle i,j \rangle} S_i S_j - J_y \sum_{\langle i,k \rangle} S_i S_k, \quad (3)$$

where J_x and J_y denote the horizontal and vertical couplings, respectively, the sums are over the horizontal ($\langle i,j \rangle$) and vertical ($\langle i,k \rangle$) nearest-neighborhood sites and the spins S_i take as usual the values $S_i = \pm 1$. We shall denote in the following with L_x and L_y the sizes of the lattice in the horizontal and vertical directions, respectively.

The corresponding partition function is

$$Z_N = \sum_S \exp \left[K \sum_{\langle i,j \rangle} S_i S_j + W \sum_{\langle i,k \rangle} S_i S_k \right], \quad (4)$$

with $K = J_x / k_B T$ and $W = J_y / k_B T$, k_B is Boltzmann's constant, and $N = L_x L_y$ is the number of sites of the lattice.

The Kramer-Wannier duality holds also for this model and has the effect of relating the two couplings (for a review see, for instance, [16,17]). The duality relations are

$$\sinh(2K^*) \sinh(2W) = 1, \quad \sinh(2W^*) \sinh(2K) = 1, \quad (5)$$

or equivalently $\tanh K^* = e^{-2W}$ and $\tanh W^* = e^{-2K}$. Denoting with $\psi(K, W)$ the free energy of the model we have

$$\psi(K^*, W^*) = \psi(K, W) + \frac{1}{2} \ln[\sinh(2K) \sinh(2W)], \quad (6)$$

from Eq. (5) we can easily obtain the self-dual line which in this case is also the critical line of the model:

$$\sinh(2K) \sinh(2W) = 1. \quad (7)$$

For $K=W$ this equation becomes the well known self-dual condition which allows us to obtain the critical temperature of the standard 2D Ising model.

All the points along this critical line correspond to the same universality class and are described in the continuum limit by the same 2D conformal field theory (CFT) with $c = 1/2$ (where c is conformal anomaly of the underlying CFT).

Outside the critical line the equation $\sinh(2K) \sinh(2W) = k$, with $k \neq 1$ constant, defines an infinite set of curves of constant temperature T in the K, W plane. In particular for $k < 1$ we have the $T > T_c$ (high-temperature) phase, while for $k > 1$ we have $T < T_c$ (low-temperature) phase, where T_c is the critical temperature of the symmetric Ising model. In the following we shall be interested in the low T phase (i.e., $k > 1$) in which the Z_2 symmetry of the model is spontaneously broken.

For reasons which will be clear below we choose different boundary conditions in the two directions: periodic boundary condition (BC) in the vertical (y -axis) direction and free BC in the horizontal (x -axis) direction. The lattice thus acquires a cylindrical geometry.¹

The most interesting feature of this model is that it can be solved exactly for any value of K and W in absence of an external magnetic field (see, for instance, [16]). Moreover an exact expression for the correlation length in the two spatial directions can be obtained in the high temperature phase by exact resummation of the strong coupling expansion [17]:

¹In the quantum field theory (QFT) interpretation of the model this choice of boundary conditions corresponds to the so-called “finite temperature regularization” of the QFT. In this framework the model describes in the continuum limit a one-dimensional QFT in contact with a heat bath whose temperature (which has nothing to do with the temperature which appears in the Hamiltonian of the model) is related to the inverse of the lattice size in the compactified direction (for a review see, for instance, [18]).

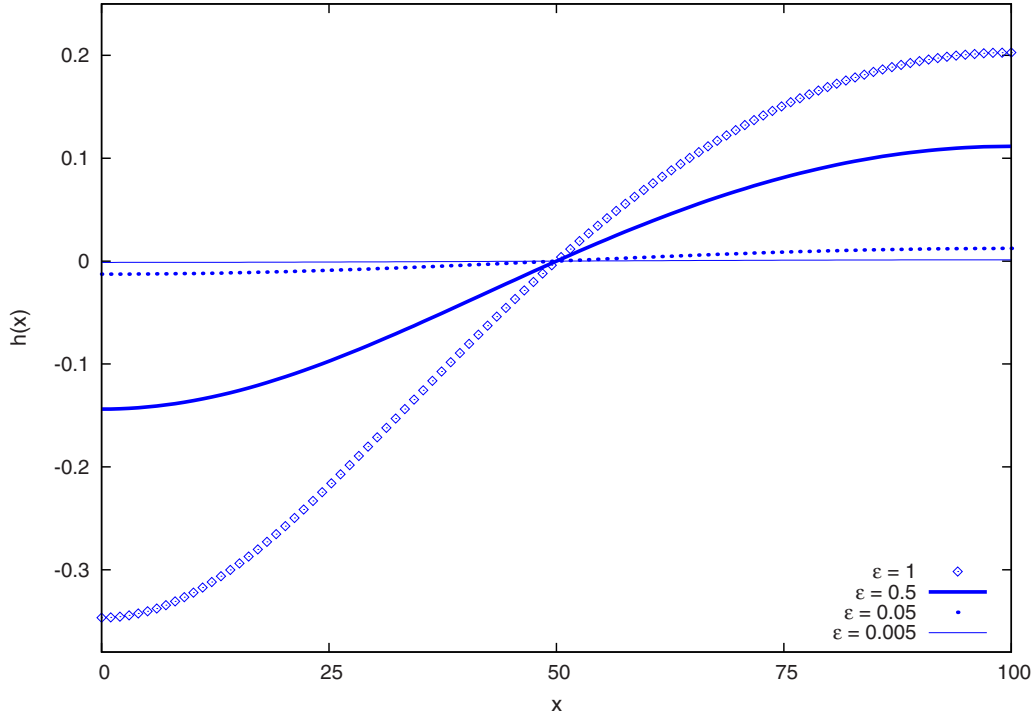


FIG. 1. (Color online) Site-dependent external magnetic field for several values of ϵ with $c=1$. On the vertical axis is reported the site-dependent external magnetic field $h(x)$ while on the horizontal axis x runs on the L_x lattice side.

$$\xi_x = -\frac{1}{\ln\left[\tanh K \frac{1+\tanh W}{1-\tanh W}\right]}, \quad \xi_y = -\frac{1}{\ln\left[\tanh W \frac{1+\tanh K}{1-\tanh K}\right]}. \quad (8)$$

From these expressions, using the duality transformation one can obtain the analogous values for the correlation length in the low T phase. This derivation however is not completely trivial. One should keep into account that in the vicinity of the critical point low and high T correlation lengths are related by an universal amplitude ratio $R_\xi \equiv \xi_+/\xi_-$, where ξ_+ and ξ_- denote the correlation lengths above and below the critical point. In the case of the 2D Ising universality class the value of R_ξ is exactly known to be $R_\xi=2$. This value keeps track of the fact that the spectrum of the underlying quantum field theory is very different in the two phases. These correlation lengths will play an important role in the following since they will allow us to evaluate the effective geometry of the model in the continuum limit.

B. Asymmetric couplings and lattice deformations

The most interesting feature of the Ising model with asymmetric couplings is that by changing the couplings along a line of constant absolute temperature, i.e., at fixed k , we can effectively modify the aspect ratio of the lattice. This is indeed a standard tool in finite temperature quantum field theory [18]. In fact it is well known in this context that we may obtain two physically equivalent regularizations of the model by squeezing the radius of the cylinder or, in a completely equivalent way, keeping the radius fixed and suitably increasing the coupling in the compactified (vertical) direction and simultaneously decreasing the coupling in the or-

thogonal (horizontal) directions. The exact amount of this change in the couplings can be determined using as physical scale the correlation length of the model. As a consequence of the changes in the couplings the vertical (i.e., along the compactified direction) correlation length ξ_y increases while the horizontal one ξ_x decreases. Since the only other scale of the problem is the circumference of the cylinder L , models with the same ratio L/ξ_y are physically equivalent. We can thus trade a change in the lattice size in the compactified direction with a change in the value of the vertical coupling. This equivalence is routinely used in lattice gauge theories and has been recently confirmed also in the context of the 2D Ising model with a set of high-precision simulations of the Binder cumulant [19]. This equivalence will allow us to construct simulation protocols in which we can change in a continuous way the radius of the cylinder (keeping the lattice size fixed and changing the couplings) thus mimicking the elongation of eukaryotic cells along the gradient of a chemoattracting potential and even the extreme situation of the formation of quasi-one-dimensional filopodia.

C. External magnetic field and metastability

In order to study the metastable behavior of the model we must add to the Hamiltonian an external magnetic field. In order to mimic an external chemotactic gradient, instead of choosing as usual an uniform external field, we choose to couple the system to a site-dependent field whose shape is plotted in Fig. 1.

The Hamiltonian considered is therefore the following:

$$H = -J_x \sum_{\langle i,j \rangle} S_i S_j - J_y \sum_{\langle i,k \rangle} S_i S_k - \sum_i h_i S_i, \quad (9)$$

which leads to the partition function

$$Z_N = \sum_S \exp \left[K \sum_{\langle i,j \rangle} S_i S_j + W \sum_{\langle i,k \rangle} S_i S_k + \beta \sum_i h_i S_i \right]. \quad (10)$$

N , K , and W as well as $\langle i,j \rangle$ and $\langle i,k \rangle$ are defined as above, $\beta = 1/k_B T$ and

$$h_i = \frac{1}{2} \ln(1 + c_i) - \frac{1}{2} \ln(1 + c) \quad (11)$$

is the external magnetic field, where

$$c_i = c \left[1 - \epsilon \cos \left(\frac{\pi x_i}{L_x} \right) \right], \quad (12)$$

where c is a constant, ϵ defines the gradient intensity of the magnetic field, and L_x is the side of the lattice along the x axis. With this definition the stable state is characterized by two phases (with minus sign for low values of x and plus sign for large values of x) separated by an interface while the metastable state, whose decay properties we shall study in the following, will be defined as the state in which all the spins are pointed in the -1 direction.

IV. CLASSICAL NUCLEATION THEORY

In this section we shall first briefly summarize the classical nucleation theory in the case of the Ising model defined on a square lattice of infinite size, then in the second part of the section we shall see the effect of introducing a finite size scale L comparable with the critical radius R_c . Most of the results reported in this section can be found in standard textbooks. For a detailed discussion see [7].

A. Infinite systems

In the classical nucleation theory the decay of the metastable state is controlled by three main physical scales: the correlation length ξ which sets the typical mean size of the droplet which are created in the system by thermal fluctuations, the critical droplet radius R_c and the size R_0 to which one droplet can grow before it is likely to meet another one. CNT usually assumes $\xi \ll R_c \ll R_0$ and from simple thermodynamic arguments allows to obtain reliable estimates for the nucleation rate and for the mean lifetime of the metastable state. Let us briefly remind the main steps of this calculation.

Let us first evaluate R_c . To keep the analysis as simple as possible we shall assume the droplet to be of circular shape with area πR^2 and perimeter $2\pi R$. It is easy to show that the analysis holds for any generic shape. The free energy of the droplet is

$$F(R) = 2\pi R \sigma_0 - \pi R^2 \Delta E, \quad (13)$$

where ΔE is the difference in bulk free-energy density between the metastable and stable states and σ_0 is the surface tension. In the Ising case in which we are interested the energy gap is proportional to the absolute value of the magnetic field $|H|$. For not too large magnetic fields a good approximation for ΔE turns out to be $\Delta E = 2MH/\beta$, where M is the spontaneous magnetization.

The probability of a fluctuation of this size is given by

$$P \sim e^{-F(R)/k_B T}. \quad (14)$$

Applying standard droplet theory arguments the critical radius is the value which minimizes Eq. (14)

$$R_c(T, H) = \frac{\sigma_0}{\Delta E}. \quad (15)$$

The nucleation rate (i.e., the probability of a critical fluctuation) is dominated by the free energy of the critical droplet $F_c = \pi \sigma_0^2 / \Delta E$:

$$I(T, H) \sim e^{-\pi \beta \sigma_0^2 \Delta E} \sim e^{-\pi \beta^2 \sigma_0^2 / 2M |H|} \equiv e^{-\Gamma/|H|}, \quad (16)$$

where we have introduced the constant $\Gamma = \pi \beta^2 \sigma_0^2 / 2M$ which keeps track of all the microscopic details of the model.

Let us discuss a few important features of this classical result.

(i) Equation (16) is only the first order in the semiclassical approximation [3–5]. The next to leading order can be evaluated using quantum-field-theory methods and leads to a prefactor whose power can be predicted analytically and agrees very well with high-precision Monte Carlo simulations (see, for instance, [20]). We shall not further discuss this issue in the present paper since for our purposes the semiclassical result will be enough.

(ii) In Eq. (16) the information about the first scale we have in the game, the correlation length of the model ξ , is hidden in the constant Γ . More precisely in the scaling region the string tension is related to ξ by the universal amplitude ratio $R_\sigma \equiv \sigma_0 \xi$ [21]. The requirement $\xi \ll R_c$ is thus translated into the condition $\Gamma \gg |H|$ and allows us to have a precise estimate of the values of H for which the CNT can be used. At the same time the $\Gamma \gg |H|$ condition implies that we should expect exponentially long nucleation times.

(iii) In the above derivation we assumed a single droplet approximation. This is a reliable choice as far as critical droplets are far enough from each other. This is the physical meaning of the condition $R_c \ll R_0$ mentioned above. It can be shown (see, for instance, [7]) that R_0 increases exponentially with $1/|H|$ thus, since $R_c \sim 1/|H|$, there will always be a value of H below which this approximation is correct.

B. Finite size systems

If we consider a system of finite size L there will always be a value of $|H|$ small enough such that $R_c > L$. In this limit the system behaves as along the coexistence line, i.e., as if $|H|$ would be negligible with respect to the other scales. Thus we can neglect the area term in Eq. (13) and the droplet free energy becomes proportional to R . The saddle-point analysis discussed above does not hold any more and one can show that instead the metastable lifetime increases exponentially with the system size L . To address this point let us define as ϕ the fraction of the system occupied by the droplet, i.e. (assuming again the simplified picture of a spherical droplet) $\phi = \pi R^2 / L^2$. Then we can rewrite the free energy as

$$F(R) \sim 2\sqrt{\pi} \phi L \sigma_0. \quad (17)$$

TABLE I. Summary of the system behavior for each value of k and ϵ . Legend: \star phase separation achieved with symmetrical couplings; \bullet phase separation achieved with asymmetrical couplings; \otimes phase separation not achieved during the simulation time, either with asymmetrical couplings.

ϵ	5	1	0.5	0.05	0.005	0.0005
$k=1.8$	$\star\bullet$	$\star\bullet$	$\star\bullet$	\bullet	\otimes	\otimes
$k=7$	$\star\bullet$	$\star\bullet$	\bullet	\bullet	\otimes	\otimes
$k=13.2$	$\star\bullet$	\bullet	\bullet	\bullet	\bullet	\otimes

As above we can trade the line tension σ_0 for the correlation length using the universal amplitude ratio R_σ and rewrite F as

$$F(R) \sim A \frac{L}{\xi}, \tag{18}$$

with $A=2\sqrt{\pi\phi}R_\sigma$ which, if we are interested in the free energy of a droplet which covers a finite fraction of the system, is a constant of order unity. Thus we see that the parameter which governs the droplet formation is actually the ratio L/ξ and that the lifetime of the metastable state increases exponentially with L/ξ .

In particular, if we are interested in a cylindrical geometry, the limiting scale will be the radius of the cylinder and, in case of asymmetric couplings, the correlation length in Eq. (18) will be the correlation length along the compactified direction.

V. SIMULATION SETTING AND RESULTS

Simulations were performed using a standard Glauber dynamics in order to mimic the local interactions of enzymes on the membrane surface [12].

We studied the model on a square lattice of sizes $L_x=L_y=L=100$. The system was initialized setting all the spins to the $S_i=-1$ value. The boundary conditions were chosen to be periodic in the y axis and free in the x axis. For definiteness we set in Eqs. (11) and (12) $c=1$ and considered six values of gradient intensity, ranging from $\epsilon=5$ to $\epsilon=0.0005$ (see Table I).

We simulated the system for three different values of k (see Fig. 2): $k=1.8(K=W=0.55)$, $k=7(K=W=0.85)$, and $k=13.2(K=W=1)$. Recall that the relation between (K, W) and k is $\sinh(2K)\sinh(2W)=k$ and $k > 1$ corresponds to the broken symmetry phase.

In order to study the effects of geometry variation on nucleation for each value of k , we smoothly changed the values of K and W from $K=W$ to the value of W and K

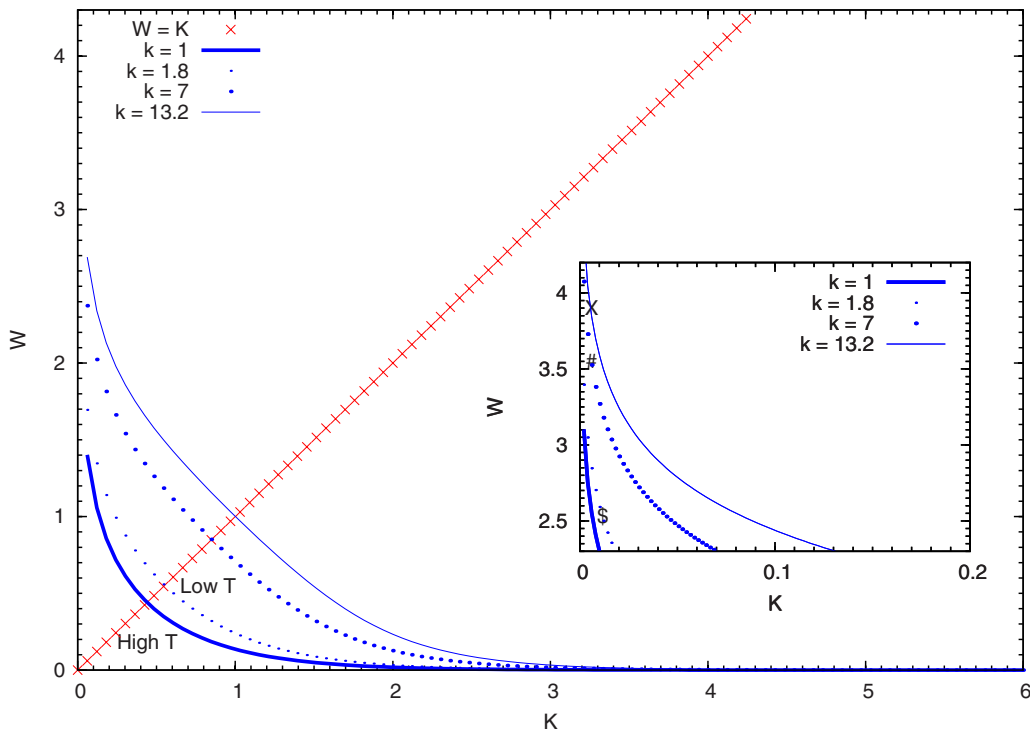


FIG. 2. (Color online). $W=\frac{1}{2}\text{asinh}(\frac{k}{\sinh(2K)})$ for several values of k . On the y and x axes are reported W and K , respectively. In the inset the points $(K; W)$ corresponding to $\xi_y=\frac{L_y}{2}$ are plotted: the symbol refers to the point $(0.0113, 2.53)$ for $k=1.8$, the # symbol refers to the point $(0.0054, 3.9)$ for $k=7$ and the X symbol refers to the point $(0.0054, 3.9)$ for $k=13.2$.

TABLE II. Summary of the details on the parameters used in the simulations. For each value of k , the K and W values are reported together with the corresponding correlation lengths ξ_x and ξ_y .

$k=1.8$				
K	0.55($\xi_x=1.225$)	0.0445($\xi_x=0.85$)	0.0225($\xi_x=0.85$)	0.0113($\xi_x=0.85$)
W	0.55($\xi_y=1.225$)	1.85($\xi_y=12.5$)	2.19($\xi_y=25$)	2.53($\xi_y=50$)
$k=7$				
K	0.85($\xi_x=0.375$)	0.0234($\xi_x=0.25$)	0.0116($\xi_x=0.25$)	0.0058($\xi_x=0.25$)
W	0.85($\xi_y=0.375$)	2.85($\xi_y=12.5$)	3.20($\xi_y=25$)	3.55($\xi_y=50$)
$k=13.2$				
K	1($\xi_x=0.29$)	0.0209($\xi_x=0.2$)	0.0108($\xi_x=0.2$)	0.0054($\xi_x=0.2$)
W	1($\xi_y=0.29$)	3.22($\xi_y=12.5$)	3.55($\xi_y=25$)	3.9($\xi_y=50$)

corresponding to $\xi_y=50=\frac{L}{2}$ (i.e., reaching a quasi-one-dimensional geometry), we let the system thermalize in this asymmetric point and then moved it back again to the symmetric $K=W$ geometry.

We checked that, for all the values of k that we studied, the results were essentially independent from the velocity of this transformation provided the thermalization time in the asymmetric points was large enough. Thus for simplicity we shall only report the results corresponding to two simulations protocols.

The first one (protocol I) corresponds to a stepwise change in the value of the couplings. More precisely we started with 5×10^3 iterations with $K=W$ in order to thermalize the system, we then changed in a stepwise way the couplings to the values corresponding to the maximal asymmetry (last column of Table II) and let the system thermalize for 5×10^4 iterations. Finally, again in a stepwise manner, we change the couplings back to the symmetric value and run the simulation for 10^4 iterations.

The second one (protocol II) corresponds to a more gradual change in the couplings. In this case, after the first 5×10^3 iterations at $K=W$, the system is gradually squeezed by simulating it for 10^4 iterations for each one of the three choices of asymmetric couplings reported in Table I. Then it is gradually moved back to the symmetric case following the same procedure and is finally allowed to thermalize again for 10^4 iterations at $K=W$.

For all the values of ϵ and k that we studied we then compared our results with those obtained by keeping the couplings (hence the geometry) unchanged (protocol III). We used this third set of simulations to identify the minimum value of ϵ detectable by the system. Details on the parameters used in the simulations can be found in Table II. All the three protocols run for exactly 65×10^3 iterations and can thus be compared among them without bias.

Due to the nontrivial shape of the external magnetic field, besides the usual magnetization $M=\frac{1}{N}\sum_i S_i$ we used the following order parameter [12] to measure the polarization degree of the system:

$$\sigma = \frac{1}{2} \frac{\sum_i^N (c_i - c) S_i}{\sum_i^N |c_i - c|}, \tag{19}$$

that is

$$\sigma = \frac{1}{2} \frac{\sum_i^N \epsilon \cos\left(\frac{\pi x_i}{L_x}\right) S_i}{\sum_i^N \left| \epsilon \cos\left(\frac{\pi x_i}{L_x}\right) \right|}. \tag{20}$$

The results of our simulations are summarized in Table I and Figs. 3–5. Let us discuss our main findings.

(i) In Fig. 3 we report the behavior of σ for three values of k and $\epsilon=0.5$ as a function of the Monte Carlo time, keeping

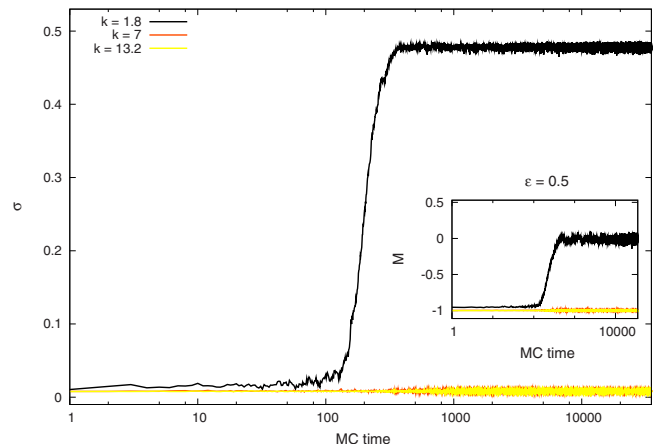


FIG. 3. (Color online) Order parameters σ and M as functions of Monte Carlo time for three values of k , $\epsilon=0.5$ and symmetrical couplings $K=W$. From the top to the bottom of the figure σ and M for $k=1.8$ in black, for $k=7$ in orange (gray) and for $k=13.2$ in yellow (light gray). The data for $k=7$ and $k=13.2$ oscillate around the same mean value.

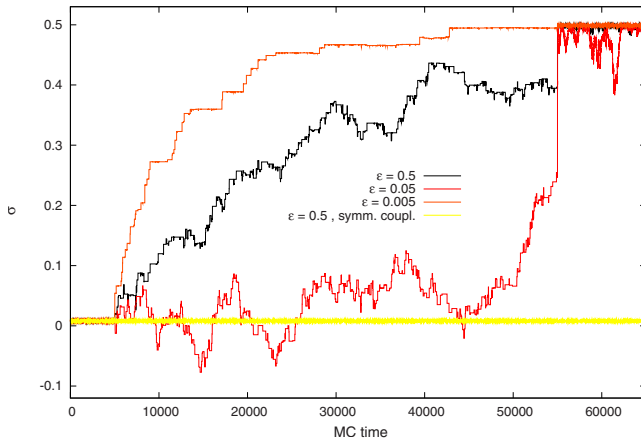


FIG. 4. (Color online) Order parameter σ as function of Monte Carlo time for $k=13.2$ and several values of ϵ for a simulation following protocol I $K=W=1$. From the top to the bottom of the figure, in orange (gray) data for $\epsilon=0.005$, in black for $\epsilon=0.5$, in red (dark gray) for $\epsilon=0.05$, and in yellow (light gray) for $\epsilon=0.5$ and symmetrical couplings.

$K=W$ (protocol III). When $K=W$, for a fixed value of ϵ the lifetime of the metastable state increases exponentially as a function of k . This is a well-known result [6] and is in agreement with classical nucleation theory. In fact as k increases the interfacial tension (and hence the free energy F_c of the critical droplet) increases. For the smallest values of ϵ and the largest values of k this time is much larger than our simulation time and as a consequence for these values of k and ϵ we did not observe a decay of the metastable state (see Table I). In our biological interpretation these values of ϵ are below the detectability threshold for the cell.

(ii) In Figs. 4 and 5 we report the behavior of σ for $k=13.2$ and several values of ϵ as a function of the Monte Carlo time for simulations following protocols I and II, respectively. By squeezing the lattice we see that the order

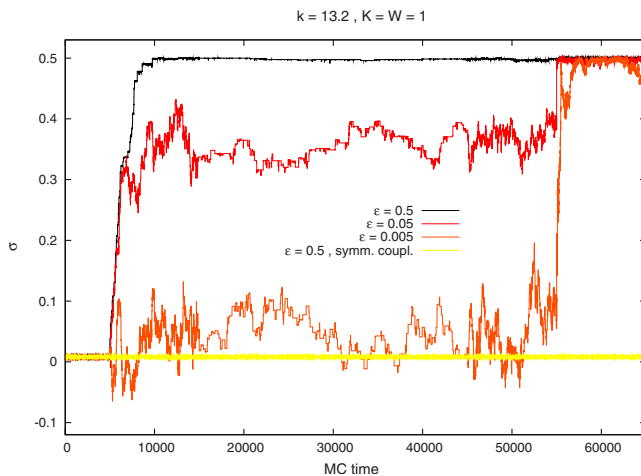


FIG. 5. (Color online) Order parameter σ as function of Monte Carlo time for $k=13.2$ and several values of ϵ for a simulation following protocol II $K=W=1$. From the top to the bottom of the figure, data for $\epsilon=0.5$ in black, for $\epsilon=0.05$ in red (dark gray), for $\epsilon=0.005$ in orange (gray), and for $\epsilon=0.5$ and symmetrical couplings in yellow (light gray).

parameter σ for the three values of ϵ reported gradually moves from ~ 0 to ~ 0.5 : i.e., at the end of the simulation the spin up cluster is exactly localized around the maximum of the magnetic field. We also report for comparison the result of the simulation with no change in the couplings. In this case due to the rather high value of k the metastable lifetime is exponentially long and in fact the order parameter keeps the value $\sigma=0$ for the whole simulation time. By gradually decreasing ϵ we could identify as $\epsilon=0.0005$ the threshold at which even with the squeezing protocol the system could not detect the external magnetic gradient. This value should be compared with the analogous value $\epsilon=0.5$ in absence of squeezing and shows that we have an enhancement of more than three orders of magnitude in the sensitivity of the system to external stimuli.

The observed behavior can be intuitively understood as follows. By changing the couplings in protocols I and II we change the value of the interfacial tension in the horizontal versus the vertical directions. This leads to the creation of asymmetric domains (vertical strips with our protocols) which play the role of nucleation drops. For large enough asymmetry these domains can wind around the vertical direction due to the periodic boundary conditions, thus leading to an effective dimensional reduction. In this regime the model behaves effectively as a one-dimensional Ising model and the vertical strips start to aggregate as it happens for the spin kinks in the 1D Ising model. This process is driven by the external field and can be very slow if the gradient ϵ is small. However, even if it may not suffice to completely polarize the lattice [see the shape of the σ parameter for the lowest ϵ values in Figs. 4 and 5], it is enough to destabilize the original metastable configuration thus allowing the system, when it is moved back to the symmetric values of couplings, to reach the stable polarized state. This is well described by Fig. 6 in which snapshots of the spin configurations are plotted at different time during the simulation, both in the symmetric case and following protocol II.

VI. CONCLUDING REMARKS

Recent studies [9–11] pointed out that chemotacting eukaryotic cells react to external chemical signals first polarizing at level of their inner membrane: the interplay between the enzymes PTEN and PI3K in the cytoplasm leads to the formation of two complementary clusters of phospholipids (PIP_2 and PIP_3) on the membrane. If the concentration of chemoattractant is larger than a threshold value, then the PIP_3 -rich cluster is localized around the maximum of the signal, determining internal cellular polarity. The above polarization is reached thanks to a phase-separation process which can be cleverly mapped on a 2D-Ising-like model mimicking a spherical cell [12]. However, dynamical geometry alterations play a pivotal role during the phase of signal caption. In particular it is well known that several types of eukaryotic cells use *filopodia*, which are quasi-one-dimensional fingerlike actin protrusions exposed at the leading edge of migrating cells, as sensors of local external environment. As very subtle directional antennas, they are sophisticated tools which allow the cell to sense teeny quan-

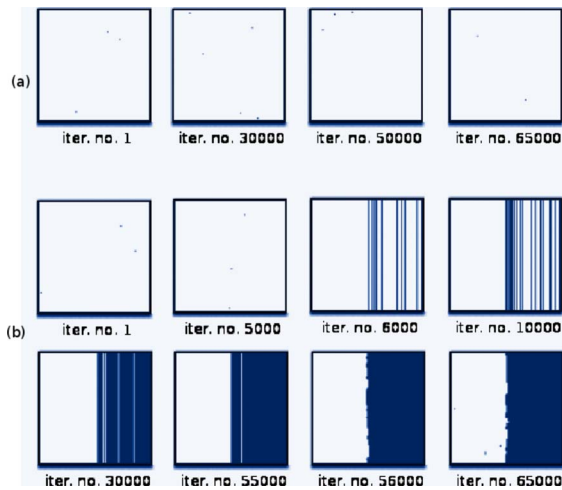


FIG. 6. (Color online) The figure shows several snapshots of a square lattice with side $L=100$ following protocol III [panel (a)] and protocol I [panel (b)]. Each snapshot is taken at a particular Monte Carlo step, indicated by the number of the corresponding iteration (iteration No. 1, iteration No. 30 000, and so on) below each square lattice. Blue (black) dots are up spins. In the panel (a), lattice with $K=W$ for the whole simulation, $k=13.2$ and $\epsilon=0.5$. In the panel (b), coarsening dynamics in presence of asymmetrical couplings between 5×10^3 and 55×10^3 iterations (from the second to the fifth lattice), $k=13.2$ and $\epsilon=0.5$.

tivity of signal otherwise negligible because below the threshold of detectability for a rigid spherical cell.

In this paper, in order to describe the phase-separation process occurring on the membrane of these filopodia we slightly modified the model proposed in [12] so as to be able

to define it on a cylindrical lattice with a radius which may change as a function of time. In order to keep the exact solvability of the model we concentrated in the $N \rightarrow \infty$ limit (see above) which corresponds to the standard anisotropic Ising model.

The main assumption behind our approach is that the phase-separation scenario proposed in [12] for the spherical cells holds also for filopodia despite their extreme geometry. This assumption is supported by a few recent works on neuronal polarization showing that the PI3-kinase and its phospholipid product PIP₃ are involved in the dendritic filopodial motility [22,23].

In particular clear evidences of a phase-separation process were observed in [23], where the authors found that focal accumulation of PIP₃ accompanies filopodial motility. In agreement with these findings we showed that squeezing the geometry of the cylinder (i.e., elongating the filopodia) allows to speed up the nucleation time even in presence of very small energy gaps between the stable and the metastable states.

Altogether our analysis and these experimental results support the idea that eukaryotic cells use conformational changes of their membrane, and in particular the protrusion of filopodia, as a tool to optimize signal detection and speed up chemotaxis even in presence of very small amounts of chemoattractants by taking advantage of the enhanced efficiency of the phase-separation process in a quasi-one-dimensional geometry.

ACKNOWLEDGMENTS

The authors would like to thank A. Gamba, L. Grassi, T. Ferraro, G. Serini, M. Osella, and L. Castagnini for useful discussions and suggestions.

-
- [1] R. Becker and W. Döring, *Ann. Phys. (Leipzig)* **24**, 719 (1935).
- [2] J. B. Zeldovich, *Acta Physicochim URSS* **18**, 1 (1943).
- [3] S. Coleman, *Phys. Rev. D* **15**, 2929 (1977).
- [4] C. G. Callan and S. Coleman, *Phys. Rev. D* **16**, 1762 (1977).
- [5] J. S. Langer, *Ann. Phys. (N.Y.)* **41**, 108 (1967); **54**, 258 (1969).
- [6] P. A. Rikvold and B. M. Gorman, in *Annual Review of Computational Physics*, edited by D. Stauffer (World Scientific, Singapore, 1994).
- [7] P. A. Rikvold, H. Tomita, S. Miyashita, and S. W. Sides, *Phys. Rev. E* **49**, 5080 (1994).
- [8] A. Zamolodchikov and A. Zamolodchikov, *Proceedings of the 33rd International Conference on High Energy Physics (ICHEP 06)*, Moscow, Russia (2006), pp. 1223–1228.
- [9] A. Gamba, I. Kolokolov, V. Lebedev, and G. Ortenzi, *J. Stat. Mech.: Theory Exp.* **2009**, P02019.
- [10] A. Gamba, I. Kolokolov, V. Lebedev, and G. Ortenzi, *Phys. Rev. Lett.* **99**, 158101 (2007).
- [11] A. Gamba *et al.*, *Proc. Natl. Acad. Sci. USA* **102**, 16927 (2005).
- [12] T. Ferraro, A. de Candia, A. Gamba, and A. Coniglio, *EPL* **83**, 50009 (2008).
- [13] D. Bray, *Cell Movements: From Molecules to Motility* (Garland, New York, 2000).
- [14] H. Guillou *et al.*, *Exp. Cell Res.* **314**, 478 (2008) (Available online at 12 November 2007).
- [15] B. Borm *et al.*, in *Proceedings of the NIC Workshop 2007*, Publication Series of the John von Neumann Institute for Computing (NIC), Vol. 36, edited by U. H. E. Hansmann, J. Meinke, S. Mohanty, and O. Zimmermann (NIC Directors, Jülich, Germany, 2007).
- [16] R. J. Baxter, *Exactly Solved Models in Statistical Mechanics* (Academic Press, London, 1982).
- [17] M. E. Fisher and R. J. Burford, *Phys. Rev.* **156**, 583 (1967).
- [18] M. Billó, M. Caselle, A. D’Adda, and S. Panzeri, *Int. J. Mod. Phys. A* **12**, 1783 (1997).
- [19] W. Selke and L. N. Schur, *Phys. Rev. E* **80**, 042104 (2009).
- [20] G. Münster and S. B. Rutkevich, *Eur. Phys. J. C* **27**, 297 (2003); G. Münster and S. Rotsch, *ibid.* **12**, 161 (2000).
- [21] A. Pelissetto and E. Vicari, *Phys. Rep.* **368**, 549 (2002).
- [22] C. Ménager *et al.*, *J. Neurochem.* **89**, 109 (2004).
- [23] B. W. Luikart *et al.*, *J. Neurosci.* **28**, 7006 (2008).